

**Proceedings for TASI 2009 Summer School on  
“Physics of the Large and the Small” :  
Introduction to the LHC experiments**

E. HALKIADAKIS\*

*Department of Physics & Astronomy, Rutgers University,  
Piscataway, New Jersey 08854, U.S.A.*

*\*E-mail: [evahal@physics.rutgers.edu](mailto:evahal@physics.rutgers.edu)  
[www.physics.rutgers.edu](http://www.physics.rutgers.edu)*

These proceedings are a summary of four lectures given at the Theoretical Advanced Study Institute in Elementary Particle Physics (TASI) in 2009. These lectures provide a basic introduction to experimental particle physics and the Large Hadron Collider experiments at CERN, with many general examples from the (still running) Fermilab Tevatron.

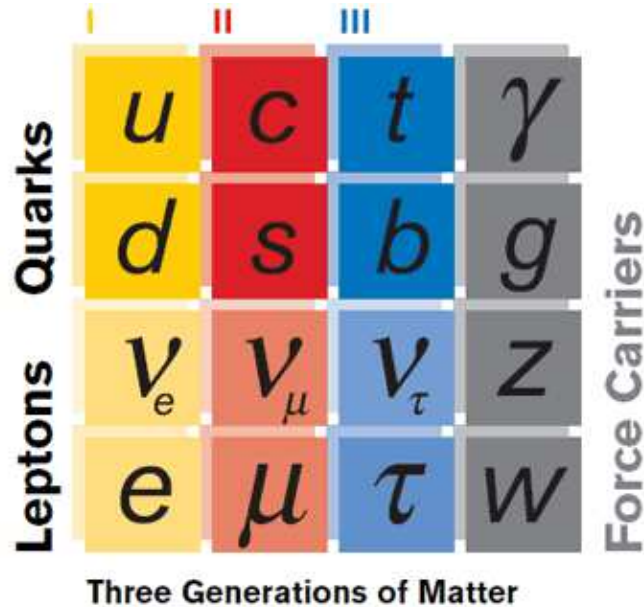
*Keywords:* Elementary Particle Physics; Collider Physics

## 1. Introduction

The Standard Model (SM) of elementary particles, summarized in Fig. 1, has been quite successful in making predictions, confirmed to incredible precision in experimental data. Yet there are still many unanswered questions about nature and the fundamental interactions. Some of today’s most challenging questions in physics are, but not restricted to:

- Is there really a Higgs boson, as predicted by the Standard Model of particle physics? If so, what is its mass?
- If not, what is the origin of electroweak symmetry breaking?
- Why is there a hierarchy of masses?
- What are the origins of dark matter and dark energy?
- Why is there no anti-matter in the universe?
- How does gravity fit into all this?

The dawn of a new energy frontier has arrived with the recent turn-on of CERN’s Large Hadron Collider (LHC). The LHC experiments at CERN use state-of-the-art technology and will hunt for answers to many of the

Fig. 1. The Standard Model.<sup>1</sup>

open questions in high energy particle physics today. From the discovery potential of the Higgs boson, to new particle and new phenomena searches, all particle physicists are focused on upcoming LHC results.

What follows is a summary of four lectures given at TASI in 2009.<sup>2</sup> These lectures provide a basic introduction to experimental particle physics, with an emphasis on CERN's LHC experiments. First, I begin with an overview of particle accelerators (Sec. 2) with an emphasis on the currently running hadron colliders, the Fermilab Tevatron and the LHC. Next, I review the importance of luminosity (Sec. 3), the proton composition (Sec. 4) and hadron collisions (Sec. 5), followed by a summary of a few key definitions every high energy physics should know (Sec. 6). I then review how particles interact with matter (Sec. 7) and how those interactions are used in designing particle detectors (Sec. 8) and the identification of particles for analysis (Sec. 9). Finally, I describe the importance of a trigger (Sec. 10), the current status of the LHC (Sec. 11), I highlight a few of the early LHC physics measurements expected (Sec. 12) and conclude (Sec. 13).

## 2. Particle Accelerators

Particle accelerators are shaped in one of two ways:

- *Linear colliders or LINAC:* An example of such an accelerator is the Stanford Linear Accelerator Center (SLAC).
- *Circular or synchrotron accelerators:* These provide higher energies than a LINAC, such as the Fermilab Tevatron.

Accelerators can also be arranged to provide collisions of two types:

- *Fixed target experiments:* When particles are shot at a fixed target. The center-of-mass energy,  $\sqrt{s}$ , for this class of experiments is:

$$\sqrt{s} = \sqrt{2 E_{beam} m_{target}} \quad (1)$$

- *Colliding beam experiments:* When two beams of particles are made to cross each other. In this case,

$$\sqrt{s} = 2 E_{beam} \quad (2)$$

Circular accelerators have been arranged to collide electrons and positrons (for example at LEP) and protons and (anti-)protons (hadron colliders). Scattering experiments have been also done by colliding leptons (electrons or positrons) and protons (for example at HERA). Examples of hadron colliders are the Tevatron at Fermilab or the Large Hadron Collider at CERN. Hadron colliders provide much higher energies than  $e^+e^-$  colliders and do not suffer from synchrotron radiation. However,  $e^+e^-$  colliders can provide us with clean environment for precision measurements.

The two currently running hadron colliders, the Tevatron and the LHC, are further described in the following sections.

### 2.1. Fermilab Tevatron

The Fermilab Tevatron, located roughly 30 miles west of Chicago, IL, accelerates protons and anti-protons to  $\sqrt{s} = 1.96$  TeV. The main ring is roughly 4 miles in circumference and when running collides 36 bunches of protons against 36 bunches of anti-protons, with roughly 100 billion particles in each bunch. Once injected, the beam is stored and the same bunches are collided typically for 20-30 hours.

The Tevatron hosts two “general purpose” experiments, the Collider Detector at Fermilab (CDF) and DO. Run I of the Tevatron lasted from 1992-1996 and in 1995 the two experiments announced the discovery of the

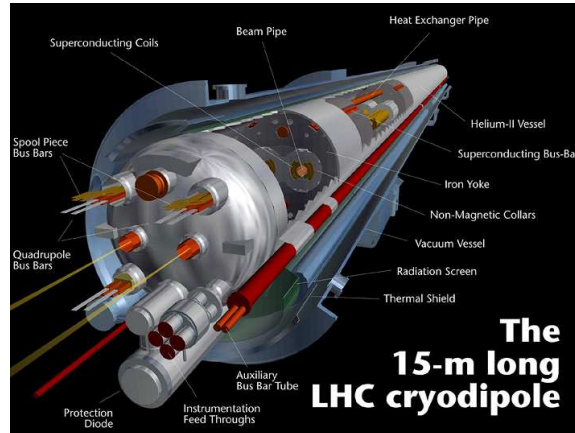


Fig. 2. Computer generated diagram of an LHC dipole magnet.<sup>3</sup>

top quark. At that point, the Tevatron entered a fixed target phase and then 2001 marked the start of Run II and will continue until at least FY2011.

## 2.2. Large Hadron Collider

The Large Hadron Collider at the CERN laboratory near Geneva, Switzerland, is a proton-proton collider with a 27 km circumference. It is designed to provide collisions with a maximum  $\sqrt{s} = 14$  TeV. In November-December 2009, the LHC turned on and collided protons at  $\sqrt{s} = 900$  GeV and for the first time at  $\sqrt{s} = 2.36$  TeV, exceeding the center-of-mass energy of the Tevatron. On March 30, 2010 the LHC achieved collisions at  $\sqrt{s} = 7$  TeV, launching a new era in particle physics. The LHC will also collide heavy ions (Pb-Pb) for shorter running periods of roughly 1 month per year.

The LHC tunnel rests 100 meters underground. The beams circle the ring inside vacuum pipes guided by super-conducting magnets. There are thousands of magnets directing the beams around the accelerator, including 1232 15 meter long, 35 ton dipole magnets shown in Fig. 2. These dipole magnets have an ingenious configuration called a “2-in-1” design allowing the two proton beams to point in opposite directions in each pipe. For a 7 TeV energy beam, the dipoles are cooled to a temperature of 1.9° K providing an 8.4 T magnetic field and a current flow of 11.7kA.

The LHC is designed to collide a maximum of 2808 proton bunches against another 2808 proton bunches. Each bunch is several cm long and contains approximately 100 billion protons. In order to increase the prob-

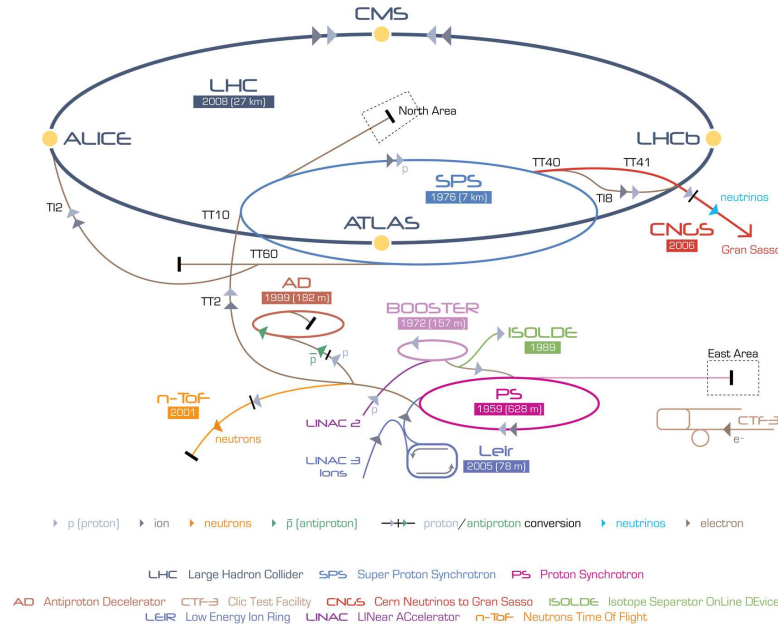


Fig. 3. The LHC accelerator chain.<sup>3</sup>

ability of a hard collision, the beam is squeezed as much as possible at the interaction point to a diameter of tens of microns. For these operating design conditions, it is expected that on average 20 additional  $pp$  interactions will occur.

The LHC accelerator chain is shown in Fig. 3. Initially, 50 MeV protons are produced in the LINAC and accelerated to 1.4 GeV in the Booster. They are then injected in the Proton Synchrotron (PS) where they reach an energy of 26 GeV and are further accelerated to 450 GeV in the Super Proton Synchrotron (SPS). Finally, they are injected in the main ring where they reach a maximum energy of 7 TeV (the maximum to-date has been 3.5 TeV per beam).

The collisions at the LHC take place at the location of the four experiments, which are:

- Compact Muon Solenoid (CMS): One of the two large “general purpose” experiments.
- A Toroidal LHC Apparatus (ATLAS): The other of the two large “general purpose” experiments.

Table 1. Comparison of the LHC and Tevatron accelerator statistics.

	LHC (design)	Tevatron (achieved)
Center-of-mass energy	14 TeV	1.96 TeV
Number of bunches	2808	36
Bunch spacing	25ns	396ns
Energy stored in beam	360MJ	1MJ
Peak Luminosity	$10^{33} - 10^{34} cm^{-2} s^{-1}$	$3.87 \times 10^{32}$ (April 2010)
Integrated Luminosity / year	10-100 $fb^{-1}$	$> 2fb^{-1}$ (2008)

- LHCb: Designed to study the  $b$ -quark sector, CP violation and rare decays.
- A Large Ion Collider Experiment (ALICE): A heavy ion experiment designed to study the nature of quark-gluon plasma.

These lectures focus primarily on the CMS and ATLAS detectors. Finally, Tab. 1 shows a summary of the LHC and Tevatron parameters for comparison.

### 3. Luminosity

Important parameters in colliders are the energy of the beams and the rate of collisions ( $R$ ), or the luminosity ( $\mathcal{L}$ ).  $R$ , is defined as:

$$R = \frac{dN}{dt} = \mathcal{L}\sigma, \quad (3)$$

where  $\frac{dN}{dt}$  is the number of hard collision events produced per second, and  $\sigma$  is the cross section of the process produced. Integrating over time, we get:

$$N_{\text{events produced}} = \sigma \times \int \mathcal{L} dt, \quad (4)$$

where  $N_{\text{events produced}}$  are the number of produced hard collision events of the process with cross section  $\sigma$  and  $\int \mathcal{L} dt$  is the integrated luminosity which is provided by the accelerator in a given time period. Unfortunately, a given high energy physics detector does not observe every collision event that is produced. For example, the trigger is inefficient, as is the identification of the final state particles, and some fraction of the events may be produced beyond the detector acceptance (see Sec. 12.1). These inefficiencies need to be experimentally evaluated and once accounted for the expression becomes:

$$N_{\text{events observed}} = \sigma \times \int \mathcal{L} dt \times \epsilon \quad (5)$$

where  $N_{\text{events observed}}$  is now the number of events observed in the detector, and  $\epsilon$  is the total efficiency of identifying the collision event of interest (see Sec. 12.1).

The units of a cross section are the same as the units of area and in high energy physics are typically represented by a barn ( $1 \text{ barn} = 10^{-24} \text{ cm}^2$ ), for example,  $mb, \mu b, nb$ , etc. The units of *instantaneous* luminosity are the same as the units of  $[1 / (\text{cross section} \times \text{time})]$ , for example  $\text{cm}^{-2} \text{ s}^{-1}$ . *Integrated* luminosity has units of  $[1 / \text{cross section}]$ , for example  $\text{cm}^{-2}$  or  $\text{pb}^{-1}, \text{fb}^{-1}$ , etc.

An example of the difference between integrated and instantaneous luminosity is shown in Fig. 4. The top figure shows the initial luminosity delivered by the Tevatron versus time and the increasing slope demonstrates the challenges of increasing the luminosity at a hadron collider. It should be noted that the instantaneous luminosity drops as the protons collide, until the next store or fill is dropped followed by (anti-)protons being re-injected and collisions resume. The bottom of Fig. 4 shows the integrated luminosity delivered by the Tevatron (black) and that acquired by the CDF experiment (purple) as a function of time; it is impossible to record every collision at a hadron collider and the difference between the two curves shows how efficiently the experiment (in this case CDF) collects the data that the accelerator delivers.

Next, let us consider an alternate expression for luminosity:

$$\mathcal{L} = f \frac{n_1 n_2}{4\pi\sigma_x\sigma_y} \approx f \frac{n_b N_p^2}{4\pi\sigma_x\sigma_y}, \quad (6)$$

where  $n_1$  and  $n_2$  are the number of particles (protons) in each of the colliding bunches,  $f$  is the frequency with which they collide,  $\sigma_x$  and  $\sigma_y$  represent the size of the transverse beam (e.g. the RMS if we assume a Gaussian shaped beam),  $n_b$  is the number of bunches and  $N_p$  is the number of particles per bunch. So in order to increase the luminosity, it is important to *squeeze* as many protons in as small a transverse beam spot as possible.

### 3.1. Exercises

- (1) Imagine a hadron collider such as the LHC or the Tevatron runs for one year with an *instantaneous* luminosity of  $10^{31} \text{ cm}^{-2} \text{ s}^{-1}$ , how much *integrated* luminosity will be delivered to an experiment?

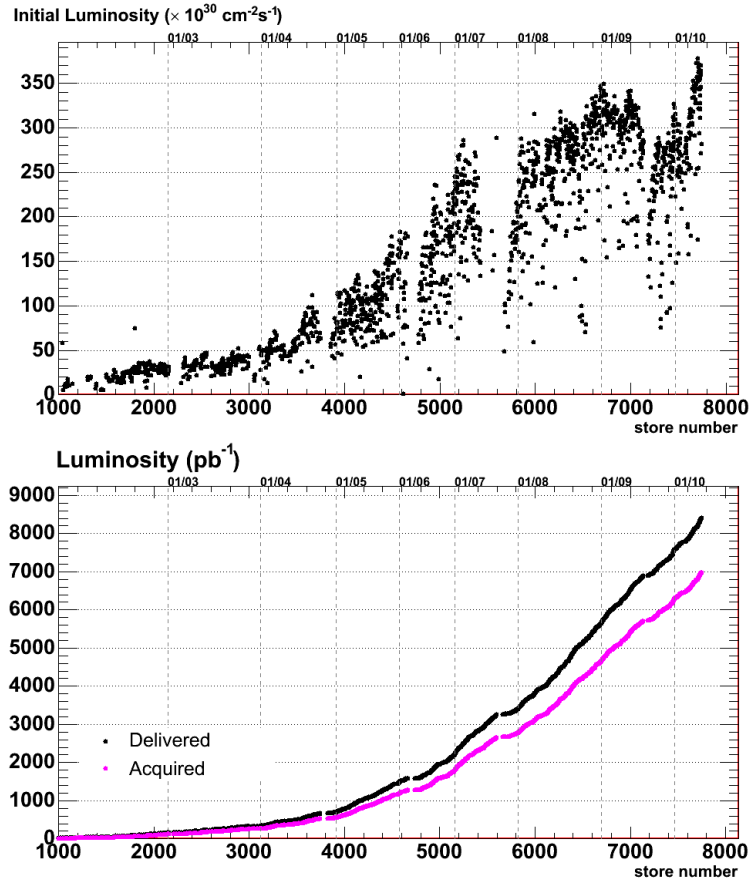


Fig. 4. Top: Initial luminosity in ( $\times 10^{30} \text{ cm}^{-2} \text{ s}^{-1}$ ) delivered by the Tevatron vs. time. Bottom: Integrated luminosity in  $\text{pb}^{-1}$  delivered by the Tevatron (black) and acquired by the CDF experiment (purple) vs. time. <sup>4</sup>

*Answer:* A year is  $3 \times 10^7$  seconds, however, accelerators do not operate every day. Assuming a good year of running is  $10^7$  seconds, we get a rough estimate:

$$\int \mathcal{L} dt = 10^{31} \text{ cm}^{-2} \text{ s}^{-1} \times 10^7 \text{ s} = 10^{38} \text{ cm}^{-2} = 10^{14} \text{ barns} = 100 \text{ pb}^{-1}$$

- (2) In  $100 \text{ pb}^{-1}$  of data, how many  $p\bar{p} \rightarrow t\bar{t}$  events will be produced at the LHC at  $\sqrt{s} = 7 \text{ TeV}$ ?

*Answer:* The  $p\bar{p} \rightarrow t\bar{t}$  cross section at 7 TeV is  $\sim 165\text{pb}$ .<sup>5</sup>

$$\begin{aligned} N_{\text{events produced}} &= \sigma \times \int \mathcal{L} dt \\ &= 165\text{pb} \times 100\text{pb}^{-1} = 16,500 \text{ } t\bar{t} \text{ pairs} \end{aligned}$$

Precisely how many events are observed depends on the efficiency of observing them in the detector.

- (3) What size beam spot is needed for  $\mathcal{L} = 1 \times 10^{34}\text{cm}^{-2}\text{s}^{-1}$  at the LHC?

*Answer:* The LHC machine frequency is  $f = c/27 \text{ km} = 11\text{kHz}$ , and is designed to contain  $n_b = 2808$  bunches and  $N_p = 1 \times 10^{11}$  protons per bunch. Substituting this into Eq. 6 above and solving for  $\sigma$  (assuming  $\sigma_x \approx \sigma_y$ ) gives:

$$\sigma_{x,y} = \sqrt{11\text{kHz} \frac{(2808)(10^{11})^2}{4\pi(10^{34}\text{cm}^{-2}\text{s}^{-1})}} = 1.5 \times 10^{-3}\text{cm} = 15\mu\text{m}$$

So we will need approximately 15  $\mu\text{m}$  beam size. For comparison, the Tevatron beam size is  $\sim 35\mu\text{m}$ .

#### 4. Proton Composition

The proton is composed of three valence quarks (two up quarks and one down quark) as well as gluons and sea quarks, but the exact composition is quite complicated. The mixture of partons inside the proton depends on the Bjorken- $x$  (the fraction of the proton's momentum carried by the parton) and  $Q^2$  (the momentum scale that characterizes the hard scattering, such as  $M^2$ , where  $M$  is the mass of the particle that is created by the scattering process). These quantities,  $x$  and  $Q^2$ , are also what parameterize Parton Distribution Functions (PDF's), as seen in Fig. 5,<sup>6</sup> which help describe the content of the proton. For low values of  $Q^2$  ( $Q^2 < 1\text{GeV}^2$ ) the proton behaves predominantly as a single particle. For a medium energy range ( $1 < Q^2 < 10^4 \text{ GeV}^2$ ), the proton interacts as a composite particle and the valence quarks dominate in the interaction. At higher energies, the gluons and sea quark PDF's are dominant. PDF's are obtained by global fits to data measurements from many experiments (deep inelastic scattering, fixed target, collider) and the constraints are summarized in Fig. 5 (green). They are essential inputs to perturbative calculations of production cross sections at hadron colliders. There are two main PDF fitting groups, CTEQ<sup>7</sup> and MRST (now MSTW),<sup>8,9</sup> which regularly provide updates to the PDF fits and their uncertainties with new data.

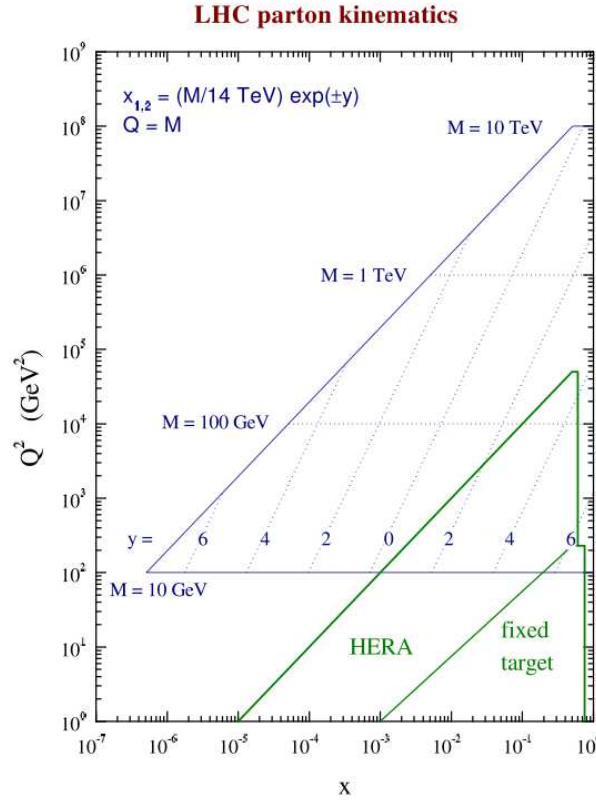


Fig. 5. PDF constraints from global fits to data shown as a function of parton variables  $Q^2$  vs.  $x$  (green). Also shown is the relationship between these parton variables and the kinematic variables for a final state produced with mass  $M$  and rapidity  $y$  assuming and LHC energy  $\sqrt{s} = 14 \text{ TeV}$  (blue).<sup>6</sup>

Figure 6 shows the PDF's vs.  $x$  for the valence quarks (up and down), sea quarks (upbar) and gluons (divided by a factor of 10). Note that the PDF's have a dramatic rise at low values of  $x$  and are dominated by gluons in that region. The valence quarks are dominant for roughly  $x > 0.1$ . Uncertainties in PDF's quantify our understanding of parton content of protons and the cross sections of processes. Therefore, making measurements which are sensitive to constraining PDF's are important since large uncertainties in PDF's result in large uncertainties in predictions and processes which are not well understood. PDF uncertainties can vary quite a lot (roughly 2-30% or more) depending on the  $x$  range and parton of interest.<sup>7-9</sup> For

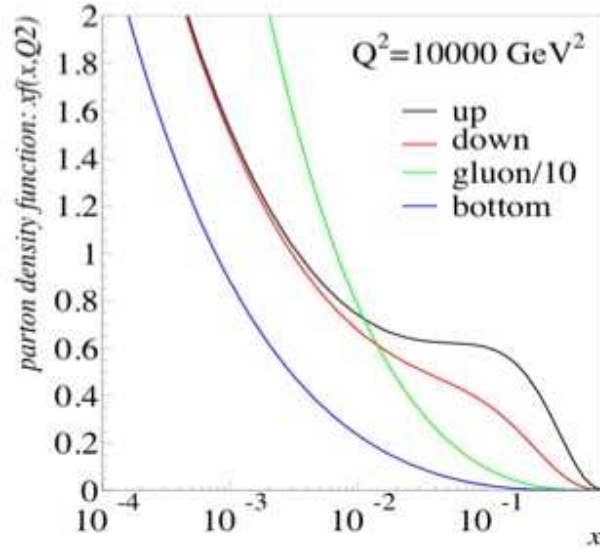


Fig. 6. PDF vs.  $x$  for up and down valence quarks, bottom sea quarks, and gluons (times 0.1) for a  $Q^2 = 10000 \text{ GeV}^2$ . The PDF's shown are CTEQ6.1M<sup>7</sup> and taken from this<sup>10</sup> useful website.

example, gluon PDF's are poorly constrained in the range approximately  $x > 0.1$ .

## 5. Hadron Collisions

The collisions, or scattering, which occurs in hadron colliders is separated into hard and soft scattering. Calculations of the hard scattering process (when two of the constituent partons in the proton collide head-on) are done using perturbative QCD. The soft processes (elastic, single diffractive, double diffractive and non-diffractive inelastic scattering) are much more difficult to understand and suffer from non-perturbative QCD effects. The majority of the total  $pp$  collisions are soft. These soft processes (everything except the hard scatter) is also generally referred to as the “underlying event”. The underlying event includes initial state radiation, final state radiation and interactions of other remnant partons in the proton. A schematic diagram describing the hard and soft processes in a hadron collision can be seen in Fig. 7. Additionally, there is a lot about the collision which we do not know, such as which partons collided with each other,

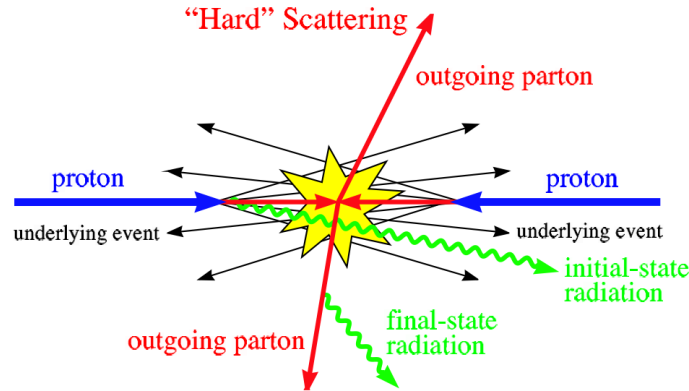


Fig. 7. Schematic of a hard scattering proton-proton collision.<sup>6</sup>

what the momentum of the partons were when they collided, and what was the effect of the other partons in the proton.

Figure 8 shows the cross sections for various SM processes as a function of  $\sqrt{s}$ . The two vertical lines at  $\sim 2$  TeV and 14 TeV represent the Tevatron and LHC energies, respectively, and note a dramatic increase in many of the cross sections for the increased  $\sqrt{s}$ . This also again emphasizes that the majority of the total inelastic cross section is coming from soft scattering processes rather than hard collisions. For example, reading from the left side of the y-axis, the total event rate produced for  $\mathcal{L} = 10^{33} \text{cm}^{-2} \text{s}^{-1}$  at the LHC is  $\sim 10^8$  events per second, whereas the event rate for  $W$  boson production is  $\sim 200$  events per second and for  $t\bar{t}$  is  $\sim 0.8$  events per second. Although there is an improved discovery potential at the LHC compared to the Tevatron, it will still be a challenge to separate out the “interesting” from the “uninteresting” events.

## 6. Definitions

In this section I outline some definitions that all high energy physicists, both theorists and experimentalists, should know.

### 6.1. Rapidity and Pseudorapidity

The *natural* coordinates of a typical collider experiment are cylindrical around the beam-pipe. If we assume the  $z$ -axis to be in the direction of

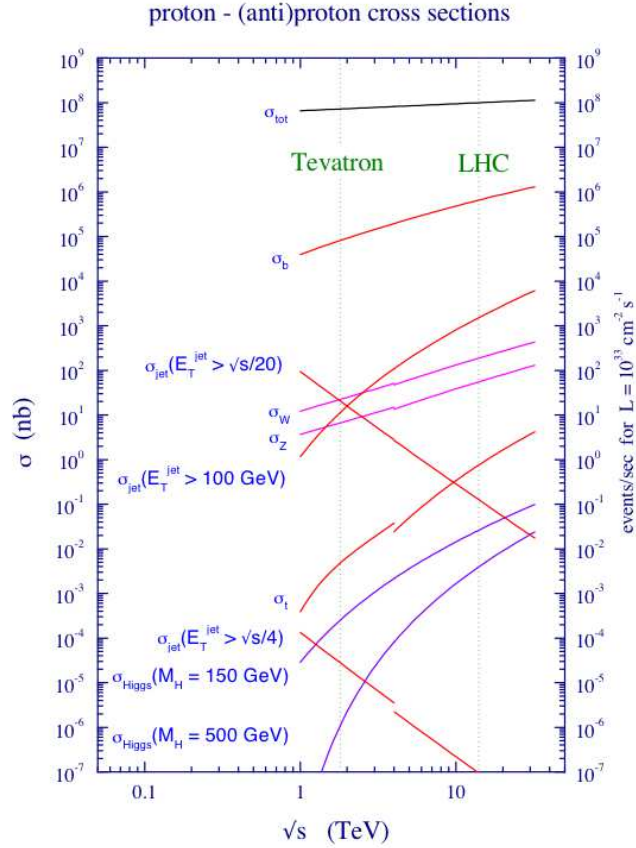


Fig. 8. Cross sections (left y-axis) and event rates (right y-axis) for SM processes for proton-(anti-)proton collisions as a function of center-of-mass energy.<sup>6</sup>

the beam, we can define  $\theta$  as the polar angle and  $\phi$  as the azimuthal angle, and  $z = 0$  is at the center of the detector or at the interaction point.

The rapidity,  $y$ , of a particle is a function of the energy,  $E$ , and the  $z$ -component of the momentum,  $p_z$  and is defined as:

$$y = \frac{1}{2} \log\left(\frac{E + p_z}{E - p_z}\right) = \tanh^{-1}\left(\frac{p_z}{E}\right). \quad (7)$$

In the coordinate system defined above, the polar angle  $\theta$  is not Lorentz-invariant. However, what we can define is the pseudorapidity,  $\eta$ , as a function of  $\theta$  as:

$$\eta \equiv -\log \tan(\theta/2). \quad (8)$$

We can then define the forward region as  $\eta \geq 1$  (or  $\theta \approx 0$ ), the backward region as  $\eta \leq -1$  (or  $\theta \approx \pi$ ) and the central region as  $\eta = 0$  (or  $\theta = \pi/2$ ).

Any change in rapidity,  $\Delta y$ , is Lorentz-invariant under boosts along the beam direction, and for a massless particle (or a nearly massless particle where  $p \gg m$ ) the rapidity and pseudorapidity are approximately equal. It is also interesting to note, that we can calculate the  $\eta$  of a particle without knowing its mass (which is very handy for experimentalists).

### 6.2. $\Delta R$ Distance

In order to determine the separation in direction between particles, experimentalists use  $\Delta R$  as a measure of “distance” and is defined as:

$$\Delta R = \sqrt{(\Delta\eta)^2 + (\Delta\phi)^2}, \quad (9)$$

where  $\Delta\eta$  and  $\Delta\phi$  are the particles’ separation in pseudorapidity and azimuthal angle, respectively. For example, this is very useful in the reconstruction of “jets”, where we use cones of  $\Delta R$  to group particles with each other; more on this in Sec. 9.

### 6.3. Transverse Quantities

Experimentalists also find it useful to focus on quantities measured in the transverse plane, or the plane perpendicular to the beam  $z$ -axis.

One quantity that is commonly used is the transverse momentum of a particle,  $p_T$ , defined as:

$$p_T = p \sin \theta. \quad (10)$$

Note that the  $p_T$  is invariant under  $z$ -boosts. Particles that escape detection (or end up in the forward region) have close to zero  $p_T$ . In this sense, the transverse plane is *opposite* of forward.

Additional transverse quantities that are often use are the transverse energy,  $E_T$ :

$$E_T = E \sin \theta, \quad (11)$$

and the transverse mass,  $m_T$ :

$$m_T^2 = \sqrt{E_T^2 - p_T^2}. \quad (12)$$

One of the most interesting and most difficult quantities for experimentalists to understand is the missing transverse energy in an event,  $\cancel{E}_T$ , defined as:

$$\cancel{E}_T \equiv - \sum_i E_T^i \hat{n}_i = - \sum_{\text{all visible}} \vec{E}_T, \quad (13)$$

where  $\hat{n}_i$  is the component in the transverse plane of a unit vector that points from the interaction point to the  $i^{\text{th}}$  calorimeter tower (see Sec. 8.2). It is an event-wide  $z$ -boost-invariant quantity and many new physics signatures are expected to show up with large  $\cancel{E}_T$ . Experimentalists also find it interesting to look at the measure of the scale of the visible  $p_T$  in an event, or  $H_T$ , loosely defined as:

$$H_T \equiv \sum_{i=\text{objects}} |\vec{p}_{T,i}|. \quad (14)$$

The definition of  $H_T$  varies since it depends on which objects (leptons, jets,  $\cancel{E}_T$ ) are included in the sum. This is also an event-wide  $z$ -boost-invariant quantity which could distinguish a SM final state from one produced by new physics.

So why are experimentalists so interested in the transverse plane? Why not look for missing  $p_z$  or missing  $E$ ? Unfortunately, in hadron collisions you do not have the luxury of knowing the initial state exactly. Remember what we said in Sec. 5, the proton itself is not what scatters. The particles that do scatter (underlying event) and escape detection have large  $p_z$  so visible  $p_z$  is not conserved and is therefore not a useful variable. However, to a good approximation the visible  $p_T$  is conserved, which is what makes it so useful.

## 7. Particle Interactions with Matter

To understand the various LHC detectors (and their differences) first requires a basic understanding of the interactions of high energy particles with matter. Particles can interact with atoms and molecules, atomic electrons and the nucleus. These interactions result in several effects such as ionization, elastic scattering, energy loss and pair-creation. There are several respectable sources on interactions of particles with matter<sup>11,12</sup> and the main one used here is the PDG.<sup>11</sup>

### 7.1. Energy Loss of Charged Heavy Particles

The primary source of energy loss of moderately relativistic heavy charged particles, such as muons, pions and protons, in matter is via ionization and atomic excitation. The average rate of energy loss is described by the Bethe-Bloch equation:

$$-\frac{dE}{dx} = Kz^2 \frac{Z}{A} \frac{1}{\beta^2} \left[ \frac{1}{2} \ln \frac{2m_e c^2 \beta^2 \gamma^2 T_{max}}{I^2} - \beta^2 - \frac{\delta(\beta\gamma)}{2} \right], \quad (15)$$

where  $z$  is the charge of the particle,  $Z$  is the atomic number of the material the charged particle is traversing,  $A$  is the atomic number of the material,  $K = 4\pi N_A r_e^2 m_e c^2$  ( $N_A$  is Avogadro's number,  $r_e$  is the classical electron radius, and  $m_e c^2$  is the mass of the electron),  $\beta$  and  $\gamma$  describe the relativistic speed of the particle,  $I$  is the mean excitation energy and  $T_{max}$  is the maximum kinetic energy of a free electron in the collision. Equation 15 is also referred to as the *stopping power*. The ionization,  $dE/dx$ , is typically expressed in terms of  $MeV/(g/cm^2)$  and is dependent on the density of the material the charge particle is traversing. The minimum ionization is found to be at a value of  $\beta\gamma \approx 3$ , and is independent of the charged particle's target.

Additionally multiple coulomb scattering off of nuclei is also an important effect for high energy charged particles since as they ionize while traveling through materials, they end up changing their direction with each interaction. The distribution of this multiple scattering is described by a Gaussian of width  $\theta_0$ :

$$\theta_0 = \frac{13.6 MeV}{\beta c p} z \sqrt{x/X_0} [1 + 0.038 \ln(x/X_0)], \quad (16)$$

where  $\beta c$  is the velocity,  $p$  is the momentum,  $z$  is the charge of the scattered particle and  $x/X_0$  is the thickness of the material in units of radiation lengths  $X_0$  (defined in Sec. 7.2). Equation 16 holds for small scattering angles, but for high scattering angles large non-Gaussian tails appear.

### 7.2. Energy Loss of Electrons and Photons and Electromagnetic Showers

Electrons primarily lose energy via bremsstrahlung and ionization. The rate at which electrons lose their energy by bremsstrahlung is nearly proportional to its energy and the rate of ionization loss rises logarithmically. There is a critical energy,  $E_c$ , at which the two loss rates are equal and it

Table 2. Radiation lengths and interaction lengths for various materials

Material	$X_0$ ( $g/cm^2$ )	$\lambda_n$ ( $g/cm^2$ )
$H_2$	63	52.4
Al	24	106
Fe	13.8	132
Pb	6.3	193

depends strongly on the absorber. For example, this critical energy for lead is 9.5 MeV.

The characteristic length that describes the energy decay of a beam of electrons is called the radiation length,  $X_0$ , defined as:

$$X_0 = \frac{716.4gcm^{-2}A}{Z(Z+1)\ln(287/\sqrt{Z})}, \quad (17)$$

where  $A$  is the atomic mass of the material and  $Z$  is the atomic number. It is the average distance the electron travels until its energy is reduced by a factor of  $1/e$  due to bremsstrahlung. By expressing the thickness in terms of  $X_0$  the radiation loss is approximately independent of the material. The amount of energy loss of electrons by bremsstrahlung is:

$$-\frac{dE}{dx} = \frac{E}{X_0}. \quad (18)$$

As is shown in Tab. 2, higher  $Z$  materials have shorter radiation lengths. For example, lead, which has a density of  $11.4 g/cm^3$  has  $X_0 = 5.5$  mm. We will see later that when designing calorimeters we want as little material as possible in front of them and high  $Z$  materials make good electromagnetic calorimeters.

The concept of a radiation length can also be applied to photons. When high energy photons lose energy in matter they do so via  $e^+e^-$  pair production. The mean free path,  $\ell$ , for pair production by a photon is:

$$\ell = \frac{9}{7}X_0. \quad (19)$$

For electrons, as we just described,  $\ell = X_0$ . So if we have a high energy photon passing through an absorber, it will produce electrons, which then radiate bremsstrahlung photons, and so on, the process repeats. This electromagnetic cascade of pair production and bremsstrahlung generate more electrons and photons with lower energy and is referred to as an electromagnetic shower. The transverse (lateral) development of electromagnetic showers scale with what is referred to as the Molière radius,  $R_M$ :<sup>11</sup>

$$R_M = 21MeVX_0/E_c, \quad (20)$$

where  $E_c$  is the critical energy as described above.

### 7.3. Hadronic Showers

Hadronic showers are produced by interactions of heavy particles with nuclei. These showers are described by the nuclear interaction length,  $\lambda_n$ :

$$\lambda_n \approx 35gcm^{-2}A^{1/3}. \quad (21)$$

For heavy, or high  $Z$ , materials the nuclear interaction length is quite a bit longer than the electromagnetic one and  $\lambda_n > X_0$  (see Tab. 2). This results in hadronic showers starting later than electromagnetic showers and are more diffuse. For example, from Tab. 2 lead, which has a density of  $\rho = 11.4 g/cm^3$ , has an interaction length of  $\sim 17$  cm.

## 8. Particle Detectors

The goal of every collider experiment is to completely surround the collision by arranging layers of different types of subdetectors. In Sec. 7 we just learned how different particles interact with matter so in order to identify them we exploit these differences. The key information of the particles that we want to extract is their momentum and charge, their energy, and their species.

Figure 9 shows schematic drawings of the CMS (top) and ATLAS (bottom) detectors, which have the traditional layered detector structure. These detectors have the following general features, starting from center moving outwards:

- *Tracking detectors within a magnetic field*: measures the charge, trajectory and momentum of charged particles
- *Electromagnetic calorimeter*: measures the energy and position of electromagnetic particles
- *Hadronic calorimeter*: measures the energy and position of hadronic particles
- *Muon chambers*: measures the trajectory and momentum (along with the tracking detector) of muons

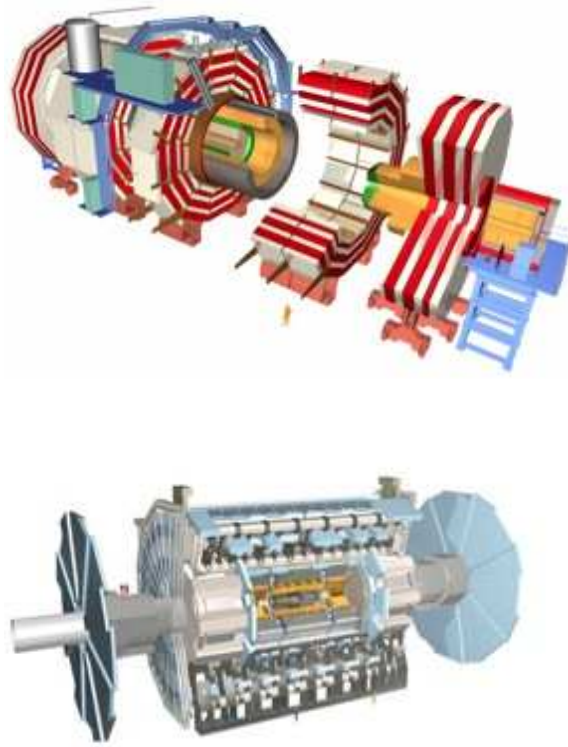


Fig. 9. Schematic drawings of the CMS (top) and ATLAS (bottom) detectors.

In the sections below I provide a brief description of these detectors, giving examples from both the LHC experiments and Tevatron experiments. Additional details on particle physics detectors can be found in these Refs.<sup>11,12</sup> . I summarize the detector technologies used in the CMS and ATLAS detectors in Sec. 8.4.

### 8.1. *Tracking Detectors*

The main goal of tracking detectors is to measure the momentum, charge and trajectory of charged particles. Ideally, we want tracking detectors to contain as little material as possible in order to minimize multiple scattering. There are two main technologies of tracking detectors in particle

physics:

- *Gas/wire drift chambers:* These devices are made of wires in a volume filled with a gas, such as Argon-Ethane. They measure where a charged particle has crossed when it ionizes the gas. There is an electrical potential applied to the wires so atomic electrons knocked off the atoms in the gas drift to a positively charged sense wire. The chamber are connected to electronics which measure the charge of the signal and when it appears. To reconstruct the tracks of the charged particles several chamber planes are necessary. Advantages to drift chambers is their low thickness (in terms of  $X_0$ ) and are the traditionally preferred technology for large volume detectors. Typical single hit resolutions range from  $\sim 100 - 200\mu m$ . An example of such a device is the CDF experiment's Central Outer Tracker (COT) <sup>13</sup> which has approximately 30,000 wires.
- *Silicon detectors:* Silicon detectors are semi-conductor detectors which are modified by doping. For example, doping with Antimony gives an n-type semiconductor or with Boron which gives a p-type semiconductor. This doped silicon is then used to create a p-n junction, to which a very large reverse-bias voltage is applied. This creates a "depletion zone" and once the silicon device is fully depleted we are left with an electric field. When charged particles cross the detector they ionize the depletion zone and create an electrical signal. Figure 10 shows a schematic drawing of a charged particle interacting in a silicon device, which has a typical thickness of  $\sim 300\mu m$ . Silicon detectors come in two varieties, either metal strips (as seen in Fig. 10) or pixels (shown in Fig. 11) which provide much higher granularity and a higher precision set of measurements. For example, the CMS silicon strip resolution ranges from  $8 - 64\mu m$  and for its pixel detector is  $\sim 15 - 30\mu m$ . Additionally, the number of pixel sensor channels at CMS is  $\sim 65$  million and at ATLAS is  $\sim 80$  million. These detectors are radiation hard and are important for detection secondary vertices (for example, from b-hadron decays as described in Sec. 9) close to the primary interaction. Silicon is now the dominant sensor material in use for tracking detectors at the LHC and especially for CMS.

Since a magnetic field is applied within the detector the momentum and charge of the particle is measured using a few points of the particle's track (trajectory) which we can use reconstruct the curvature of the track. The transverse momentum ( $p_T$ ) of charged particles is proportional to the

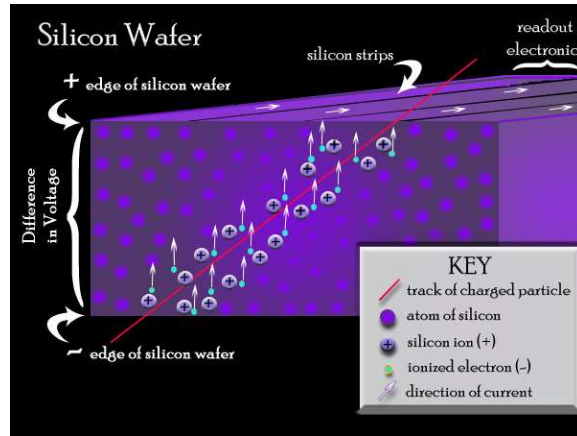


Fig. 10. Schematic of a silicon semiconductor detector.<sup>14</sup>

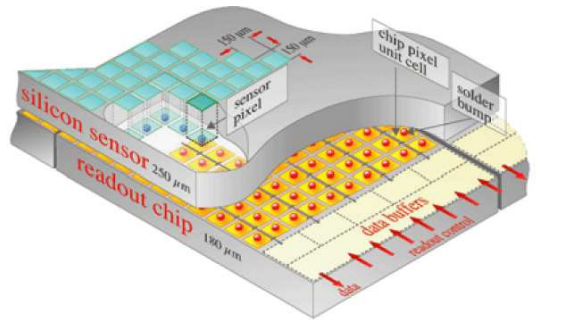


Fig. 11. Schematic of the silicon pixel detector at CMS.<sup>15</sup>

radius of curvature and to the  $B$  field. In particular,

$$p_T = 0.3 q B r, \tag{22}$$

where the reconstructed track  $p_T$  is measured in  $\text{GeV}/c$ ,  $B$  is in Tesla, the total particle charge is  $qe$  ( $e$  is the magnitude of the electron charge) and  $r$  is measured in meters and is the radius of curvature of the track.

## 8.2. *Electromagnetic and Hadronic Calorimeters*

Electromagnetic calorimeters are designed to measure the energy of electromagnetic particles (both charged and neutral) and their position. This is done by constructing them using a heavy, high  $Z$  material to initiate an electromagnetic shower, as described in Sec. 7.2, to totally absorb the energy and stop the particles. The important parameter for the material used in electromagnetic calorimeters is the radiation length  $X_0$ , and have typical values of 15-30  $X_0$ . Additionally, it is key to have as little material before the calorimeter as possible (this means the tracker) so that the particles do not radiate before they reach it.

The relative energy uncertainty (or resolution),  $\sigma_E$ , of calorimeters decreases with the energy  $E$  of the particle and can be parameterized as follows:

$$\frac{\sigma_E}{E} = \frac{a}{\sqrt{E}} \oplus b \oplus \frac{c}{E}, \quad (23)$$

where  $a$  is referred to as the stochastic term and quantifies statistics related fluctuations,  $b$  is the constant term and  $c$  is primarily due to noise (for example, in the electronics). The three terms in Eq. 23 are added in quadrature (denoted by the symbol  $\oplus$ ).

There are two types of calorimeter detectors:

- *Homogeneous calorimeter*: These detectors are generally made of an inorganic heavy, high  $Z$  material which is also scintillating. The idea is to create an entire volume to generate the electromagnetic signal, as seen in Fig. 12 (top). Examples of these calorimeters include a variety of crystals such as CsI, NaI, and PbWO, and ionizing noble liquids such as liquid Ar. Energy resolutions of these types of detectors are typically  $\frac{\sigma_E}{E} \sim 1\%$ .
- *Sampling calorimeter*: These calorimeters are made of an active medium which generates signal and a passive medium which functions as an absorber as seen in Fig. 12 (bottom). Examples of active medium materials are scintillators, ionizing noble liquids, and a Cherenkov radiator. The passive material is one of high density, such as lead, iron, copper, or depleted uranium. Energy resolutions of sampling calorimeter detectors are typically  $\frac{\sigma_E}{E} \sim 10\%$ .

The scintillating light created in calorimeters is interpreted as a signal using photo-multiplier tubes (PMT's) and translated as the energy of the particle.

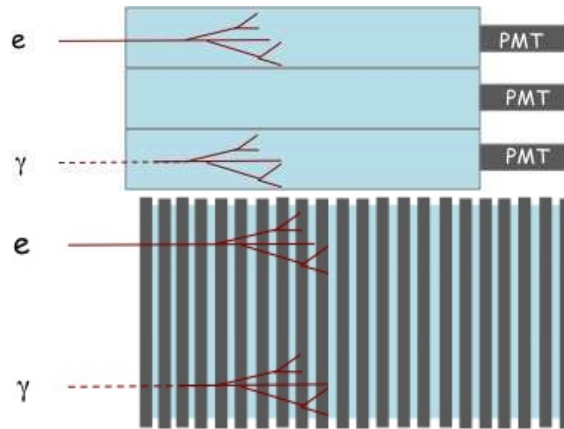


Fig. 12. Schematics of a homogeneous calorimeter (top) and a sampling calorimeter (bottom).

The purpose of hadronic calorimeters is to measure the energy of heavy hadronic particles. Hadronic calorimeters are similar to electromagnetic calorimeters but in this case the important parameter of the absorber is the interaction length  $\lambda_n$ . In general, a hadronic calorimeter has  $\lambda_n \approx 5 - 8$ . They typically are sampling calorimeters and tend to be larger and coarser in sampling depth than electromagnetic calorimeters, and therefore have larger energy resolutions. For example, the stochastic term is usually in the 30-50% or even higher.

### 8.3. Muon Chambers

Recall that the muon signature is that of a minimum ionizing particle and extraordinarily penetrating and therefore the detectors for identifying them are the outer-most layer of a collider detector. These detectors are made up of several layers of tracking chambers as described in Sec. 8.1. Their primary purpose is to measure the momentum and charge of muons. The measurements from the muon chambers are combined with the tracks reconstructed with the inner tracker to fully reconstruct the muon trajectory.

Muon chambers in LHC experiments are made from a series of different types of tracking chambers for precise measurements and some examples include:

- Drift Tubes (DT's): Wire chamber devices, so when muons traveling through kick off atomic electrons in the gas and drift to the positively

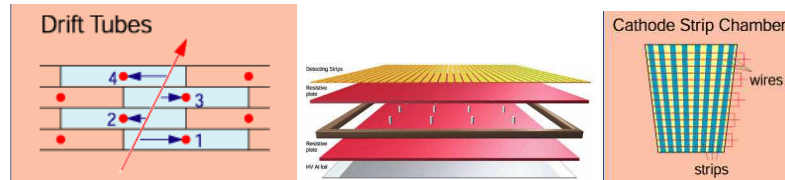


Fig. 13. Examples of Muon Chambers in the LHC experiments.<sup>16</sup> From left to right: Drift Tubes, Resistive Plate Chambers and Cathode Strip Chambers.

charged wire.

- Cathode Strip Chambers (CSC's): Wires crossed with metallic strips in a gas volume, so when muons traverse the detectors electrons drift to the positively charged wire as described above. Additionally, the positive ions in the gas drift to the metallic strips and induce a charged pulse perpendicular to the wire, giving a two dimensional coordinate of the traveling muon.
- Resistive Plate Chambers (RPC's): Oppositely charged parallel plates containing a gas volume, creating drift electrons when muons cross the detector.

Schematic drawings of DT's, RPC's and CSC's are shown in Fig. 13.

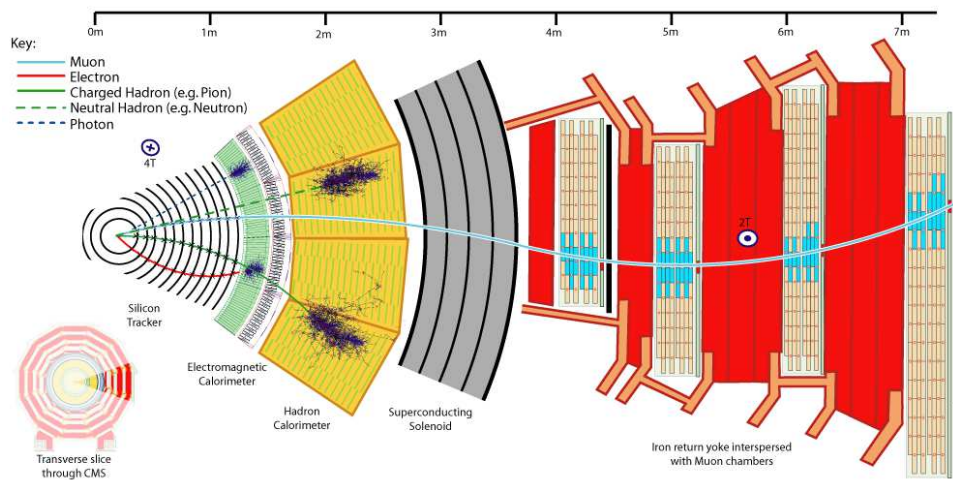
#### 8.4. The ATLAS and CMS Detectors

In this section I give a brief summary of the details of the CMS and ATLAS detectors shown in Fig. 9. Additional detailed information can be found in the technical design reports (TDR) <sup>17-20</sup> for the two experiments.

Both the CMS and ATLAS detectors are large scale experiments in every sense. CMS is 21 m long, 15 high m and 15 m wide and weighs 12,500 tons. The dimensions of ATLAS are even larger, 46 m long, 25 m high and 25 m wide, and weighs 7000 tons. CMS is located at Point 5 around the LHC ring in Cessy, France, whereas ATLAS is located at Point 1 and is in Meyrin, Switzerland (see Fig. 3). Due to the high intensity of the collisions the detectors will experience, they both have been designed to be very radiation hard, in particular the tracking detectors closest to the beam-pipe. The ATLAS and CMS experiments have designed their subdetectors using different approaches and a summary of the detector technologies used is shown in Tab. 3.

Table 3. ATLAS and CMS Subdetectors

Detector	ATLAS	CMS
Tracking	silicon/gas	silicon
EM Cal	liquid Argon	PbWO
HAD Cal	steel/scintillator	brass/scintillator
Muon	RPC's/drift	RPC's/drift
Magnet	Solenoid (inner) / Toroid (outer)	Solenoid
B Field	$\sim 2$ T / $4$ T	$\sim 2$ T

Fig. 14. Transverse slice of the CMS detector, showing the identification of particles.<sup>21</sup>

## 9. Particle Identification

In this section, I describe how these detectors described in Sec. 8 are used for particle identification. Figure 14 shows a schematic of a transverse slice of the CMS detector outlining the identification of various particles. One may find it useful to refer to this diagram while reading the description below.

- *Electrons and Photons:* Electrons are identified as an energy deposit in the electromagnetic calorimeter, and is required to have a shower shape (energy loss) consistent with an electromagnetic shower. It is also required to have little or no energy in the hadronic calorimeter. Since electrons are charged particles it needs to be associated with a track reconstructed in the tracker, and is therefore required to have a matched position measurement in the calorimeter with the one from

the track. If the electromagnetic cluster of energy does not have a track pointing to it then it becomes a candidate for being a photon.

- *Muons*: Muon identification begins by reconstructing a track in the muon system which is then matched with a track in the inner tracker. Additionally, since muons are minimum ionizing particles, they are expected to deposit little or no energy in the calorimeters.
- *Jets*: Jets are created when a quark or gluon is knocked out of the proton and due to parton confinement subsequently a hadron is created. This hadron forms a jet once it decays and fragments into many particles (hadronization), which are essentially collimated object. The reconstruction of a jet is the experimentalists representation of a parton. There are several algorithms for reconstructing jets but overall what these reconstruction algorithms do is attempt to group the particles from the hadronization process together and measure the energy of the parton. There are two main categories of jet algorithms that experimentalists and theorist use to reconstruct jets: (1) Cone algorithms<sup>22</sup> when one draws circles of  $\Delta R$  around clusters of energy according to some rule, and (2) Recursive cluster reconstruction such as the anti- $k_T$  algorithm<sup>23</sup> which is now the default jet algorithm of choice for the LHC experiments.

Measuring the jet energy has several challenges since it is impossible to determine which particles came from which hadronization process. There are several effects which contribute to the complication of the jet energy measurement, such as multiple  $pp$  interactions, spectator partons interacting and noise in the calorimeters. However, experimentalists have ways of correcting for such effects and this calibration the jet energy is generally called the Jet Energy Scale (JES) and often depends on the  $p_T$  and the  $\eta$  of the jet.

- *b-hadrons*: There is a special category of jets coming from  $b$  hadrons which are long-lived (with  $c\tau \sim 450\mu m$ ) and massive. There are two standard techniques for identifying a  $b$  hadron decay, referred to as *b-tagging*. One can look for displaced tracks forming a secondary vertex away from the primary vertex of the interaction. Alternatively one can identify soft leptons (electrons or muons) inside the jet, which would be a signature specific to semi-leptonic  $b$  decays.
- *Tau Leptons*: The identification of tau leptons is for hadronically decaying taus, which decay  $\sim 49\%$  of the time to a single charged hadron and neutrinos and  $\sim 15\%$  of the time to three charged hadrons and neutrinos. Leptonically decaying taus are indistinguishable from “normal”

electrons and muons. The reconstruction algorithms for taus assume that taus form narrow jets in the calorimeter. First one forms a  $\Delta R$  cone around clusters of energy and tracks (a signal cone) and a second larger  $\Delta R$  cone around the signal cone (an isolation cone) where there is little or no calorimeter and track activity. In the signal cone, one or three tracks are required as well as electromagnetic energy in the calorimeters from neutral particles (such as  $\pi^0$ s).

- *Neutrinos or  $\cancel{E}_T$* : Neutrinos are weakly interacting particles and pass through all the material in the LHC detectors. They are identified indirectly by the imbalance of energy in calorimeters. This missing energy was previously defined above in Eq. 13 and recall that it is one of the most interesting and most difficult quantities for experimentalists. Various effects could contribute to the complications of the  $\cancel{E}_T$  measurement such as dead calorimeter cells or a jet whose hardest hadron enters a crack (between cells) in the calorimeter or an improperly calibrated calorimeter. Therefore, we need to carefully understand this quantity as it is very important for searches of new physics processes which could produce additional weakly interacting particles.

## 10. Selecting and Storing the Interesting Events: Trigger and Computing

At design a center-of-mass energy of 14 TeV and a luminosity of  $10^{33} \text{ cm}^{-2} \text{ s}^{-1}$ , Fig. 8 shows that the total cross section at the LHC will be  $\sim 10^8$  nb. The rate for all collisions will be around 40 MHz. Since it is not possible to record every collision event, quick decisions need to be made *a priori* selecting the interesting events worthy of analysis. This filter, or trigger, needs to single out rare processes and reduce the common processes. We also want to keep less interesting events for “standard-candle” measurements (such as jet and  $W$  boson and  $Z$  boson production cross sections), calibrations, and so on. It is critical to consider carefully the make-up of the trigger and make wise choices, otherwise the events will be thrown away forever.

A *typical* trigger table will contain triggers on: electroweak particles (photons, electrons, muons, taus) at as low an energy as possible, very high-energy partons (jets), and apparent invisible particles ( $\cancel{E}_T$ ). Theory very often plays a role in guiding these choices, therefore it is important to have good communication between theorists and experimentalists.

The LHC experiments have two levels of triggers, one which bases its decision on hardware electronics (L1), and a second level which based on

software programming (the high level trigger or HLT). Recall, the starting trigger rate is 40 MHz, which gets reduced after the L1 trigger to a rate of around 100kHz. The HLT trigger further prunes this down to roughly 150-200 Hz, which is the event rate that the experiments record. Therefore, the final decision of the trigger is to keep  $\sim 1/200,000$  events occur every second, there is no room for mistakes.

One should be very aware that all measurements are distorted by the trigger selection thresholds and any measurement must account for the efficiency of the trigger and that resulting distortion. Therefore, it is necessary to include “backup” or “monitoring” trigger for measuring the efficiencies of the more interesting triggers to be used for physics analysis. Additional details on the ATLAS and CMS trigger and data acquisition systems can be found in Refs. <sup>17-20</sup>

The LHC will produce roughly 15 petabytes (15 million gigabytes) of data annually. Finally, there is the challenging task of distributing the recorded data around the world for analysis. The LHC has a tiered computing model to distribute this data around the world, referred to as the Grid.<sup>24</sup>

## 11. Status of the LHC

These TASI lectures were given in June 2009 and the LHC has since turned on and the experiments have been collecting data. It was on November 20, 2009 when the LHC first came back online, circulating proton beams of 450 GeV and three days later the beams collided for the first time at  $\sqrt{s} = 900$  GeV. Then in December, protons collided for the first time ever at  $\sqrt{s} = 2.36$  TeV, exceeding the center-of-mass energy of the Tevatron. And on March 30, 2010 the LHC achieved again the highest ever energy collisions at  $\sqrt{s} = 7$  TeV, and a new era in particle physics commenced. Since then the machine and the experiments have been running smoothly and has so far achieved a luminosity around  $10^{27} \text{ cm}^{-2} \text{ s}^{-1}$ , with a goal of  $\sim 10^{32} \text{ cm}^{-2} \text{ s}^{-1}$ . The plan is to continue running the accelerator at  $\sqrt{s} = 7$  TeV through 2011 (with a short technical stop at the end of 2010) until it has delivered  $> 1 \text{ fb}^{-1}$  of good collision data to the experiments. This dataset will be enough to make potentially very exciting new discoveries in the near future.

## 12. Early LHC Physics Measurements

With the initial data from the LHC, in order to have confidence of any potential claims of discovery, the very first job of the experimentalists is to understand the detector. The early LHC measurements will be focused on calibrating, and aligning the detector as well as rediscovering the SM since it is the SM particles which are the only ones we are *guaranteed* to see. A complete list of expectations for physics measurements from the CMS and ATLAS experiments can be found in their TDR's<sup>18–20,25</sup> and updated results located at the experiment websites.<sup>21,26</sup>

Here I will only list a few examples of early LHC physics measurements of SM processes. Without measurements such as the ones listed below, we can not be assured of any claims of discovery of new physics.

- Charged track track multiplicity: This measurement has already been made by the ALICE,<sup>27</sup> CMS<sup>28</sup> and ATLAS<sup>29</sup> experiments with the recently collected 900 GeV and 2.36 TeV data.
- Inclusive jet cross section
- $Z$  and  $W$  boson production cross sections
- $t\bar{t}$  pair production cross section

In the next section, I will highlight a few of the key elements which go in making an example measurement such as a production cross section.

### 12.1. *Example Analysis: Measuring a Cross Section*

Measurements of the production cross sections of known processes produced in high energy  $pp$  collisions provide important tests of the SM. Although the measurement of a cross section is primarily a counting experiment, one should not be fooled into thinking it is a simple analysis; it is actually rather complex with many ingredients which need detailed understanding. Experimentally, the cross section for a process of interest is measured as:

$$\sigma = \frac{N_{obs} - N_{bkg}}{\int \mathcal{L} dt \times \epsilon}, \quad (24)$$

where  $N_{obs}$  is the number of observed candidate events selected in the data sample,  $N_{bkg}$  is the estimated number of background events mimicking the signal,  $\int \mathcal{L} dt$  is the integrated luminosity of the data sample analyzed, and  $\epsilon$  is the overall efficiency of observing the produced events of interest.

The evaluation of the background processes which *fake* your signal can often be a difficult task. In general, backgrounds are evaluated using a com-

bination of Monte Carlo simulations of select processes (such as electroweak production) and evaluating them directly from the data (for example, jets *faking* leptons).

The total efficiency,  $\epsilon$ , typically has several components. Overall, one needs to evaluate:

$$\epsilon = \frac{\text{Number of events used in the analysis}}{\text{Number of events produced}}. \quad (25)$$

Some of the key ingredients to evaluating the total efficiency are the product of:

- *Trigger efficiency*: Modeling of the trigger in collider experiments has been found to be quite complex. Generally, trigger efficiencies are obtained from data, measuring the efficiencies of the different components that make up a particular trigger from an other trigger with looser requirements. These efficiencies can have a dependence on  $p_T$  or  $\eta$  for example and a trigger turn-on curve as a function of these variables need to be evaluated.
- *Particle identification efficiency*: The identification of the final state particles as described in Sec. 9 are often not highly efficient. One needs to determine how often an object that should have been identified failed the selection criteria. The identification efficiencies are generally obtained from data. For example, for leptons,  $Z \rightarrow \ell\ell$  decays are ideal for measuring their efficiencies.  $Z$  boson decays provide a clean environment and a precisely known mass resonance. The efficiencies are then measured by selecting  $Z$  candidate events where only one of the leptons is rigorously identified, while the other lepton has its selection criteria significantly loosened, and then counting how often the loose lepton fails the full selection.
- *Reconstruction efficiencies*: Again, experimentalists rely on the data to help them evaluate the efficiency of the reconstruction of tracks, the reconstruction of clusters in the calorimeters, etc.
- *Kinematic acceptance*: An additional ingredient to knowing the total efficiency  $\epsilon$  is also knowing the fraction of the decays which satisfy the geometric constraints of the detector (for example  $\eta$  coverage) and the kinematic constraints (for example  $E_T$  or  $p_T$  of the final state objects) of the event selection criteria. The acceptance is primarily determined from a Monte Carlo simulation of the signal process.

There are a lot of examples of cross section measurements in the available literature which describe in detail the complexities of the analysis, and

I provide a reference to rather complete one of the inclusive  $W$  and  $Z$  cross sections at the Tevatron<sup>30</sup> for further reading.

### 13. Concluding Remarks

With the startup of the LHC, we are at the dawn of a new era of particle physics. In these lectures, I was only able to touch the surface of the challenges experimentalists face when trying to understanding the data to the point of confidently making a discovery. With these lectures I provide a starting point for understanding the physics of how particles interact with matter<sup>11,12</sup> and how we exploit those interactions in the state-of-the-art CMS and ATLAS detectors<sup>17-20</sup> to be used in analyses. It is a great time to be working on the energy frontier as we are all looking forward to upcoming discoveries at the LHC.

### 14. Acknowledgments

I would like to thank the TASI organizers for their hospitality and for their kind invitation to give these lectures. It was a wonderful opportunity and I hope I interact again in the near future the highly enthusiastic group of students who attended the lectures. Their energy was refreshing and I encourage them to continue to have lively discussions with experimental colleagues.

### References

1. <http://www.symmetrymagazine.org/images/200502/standard3.gif>.
2. [https://physicslearning2.colorado.edu/tasi/tasi\\_2009/tasi\\_2009.htm](https://physicslearning2.colorado.edu/tasi/tasi_2009/tasi_2009.htm).
3. <http://cdsweb.cern.ch/>.
4. <http://www-cdf.fnal.gov/>.
5. N. Kidonakis, “Higher-order corrections to top-antitop pair and single top quark production”, arXiv:hep-ph/0909.0037.
6. J.M. Campbell, J.W. Huston, W.J. Stirling, Rept. Prog. Phys. **70**, 89 (2007). Also, see arXiv:hep-ph/0611148.
7. J. Pumplin, D.R. Stump, J. Huston, H.L. Lai, S. Kuhlmann, J.F. Owens and W.K. Tung, J. High Energy Phys. **0310**, 046 (2003).
8. A.D. Martin, W.J. Stirling, R.S. Thorne and G. Watt, Phys. Lett. B **652** 292 (2007).
9. A.D. Martin, W.J. Stirling, R.S. Thorne, G. Watt, “Parton distributions for the LHC”, arXiv:hep-ph/0901.0002.
10. <http://durpdg.dur.ac.uk/hepdata/pdf3.html>.
11. C. Amsler *et al.* (Particle Data Group), “The Review of Particle Physics”, Physics Letters B667, 1 (2008) and 2009 partial update for the 2010 edition.

12. W. R. Leo, *Techniques for Nuclear and Particle Physics Experiments*, 2nd edn. (Springer, 1994).
13. T. Affolder *et al.*, Nucl. Instrum. Meth. **A526** 249 (2004).
14. [http://www-cdf.fnal.gov/virtualtour/silicon\\_detector.html](http://www-cdf.fnal.gov/virtualtour/silicon_detector.html).
15. <http://cms.web.cern.ch/cms/Detector/Tracker/index.html>.
16. <http://cms.web.cern.ch/cms/Detector/Muons/index.html>.
17. “CMS Physics TDR: Volume I, Detector Performance and Software”, CERN-LHCC-2006-001.
18. <http://cmsdoc.cern.ch/cms/cpt/tdr/>.
19. “ATLAS TDR: Detector and Physics Performance Technical Design Report”, CERN-LHCC-1999-14/15.
20. <http://atlas.web.cern.ch/Atlas/internal/tdr.html>.
21. <http://cms.cern.ch/>.
22. G.C. Blazey *et al.*, “Run II jet physics”, arXiv:hep-ex/0005012.
23. M. Cacciari, G. P. Salam, G. Soyez, J. High Energy Phys. **04**, 063 (2008).
24. <http://lcg.web.cern.ch/lcg/>.
25. “CMS Physics TDR: Volume II, Physics Performance”, CERN-LHCC-2006-021, J. Phys. G, **34**. 995 (2007).
26. <http://atlas.ch/>.
27. The ALICE Collaboration, Eur.Phys.J. **C65**, 111 (2010).
28. The CMS Collaboration, J. High Energy Phys. **02**, 041 (2010).
29. The ATLAS Collaboration, arXiv:hep-ex/1003.3124.
30. A. Abulencia *et al.*, J. Phys. G: Nucl. Part. Phys. **34**, 2457 (2007).